Microsyst Technol (2010) 16:317–331
DOI 10.1007/s00542-009-0909-z

TECHNICAL PAPER

Robust dual-stage and repetitive control designs for an optical pickup with parallel cantilever beams powered by piezo-actuation

Paul C.-P. Chao · Lun-De Liao · Hsing-Hung Lin · Ming-Hsun Chung

Received: 4 August 2008 / Accepted: 14 July 2009 / Published online: 19 August 2009

Abstract This study proposes a dual-stage lens actuator used for optical disc drives, which includes a piezoceramic parallel-beam as a fine actuator and a voice coil motor (VCM) as the coarse one. The positioning algorithm of the objective lens is comprised of robust H_∞ fine/coarse controllers designed based on μ synthesis and a repetitive controller to further reduce effects of disturbance. To these ends, the dynamic model of the piezoceramic parallel-beam and VCM are first established and then identified by experiments. Based on these identified models, the system dynamics is represented as a standard form, which is ready for μ synthesis to design robust controller. Performing optimization, the desired robust H_∞ controller used for conducting fine/coarse positioning is obtained. In addition to H_∞ control design, the repetitive controller is further forged to reduce the effect of disturbance based on the periodic nature of the disturbance. Simulations and experiments are conducted to validate the performance expected by previously designed controllers. The experiment shows that the fine piezo-actuator bears the responsibilities of compensating in-precision positioning of the coarse VCM actuator and external small level periodic disturbance.

P. C.-P. Chao (✉)
Institute of Imaging and Biophotonics, Department of Electrical and Control Engineering, National Chiao Tung University, Hsinchu 300, Taiwan
e-mail: pchao@mail.nctu.edu.tw

L.-D. Liao · H.-H. Lin
Department of Electrical and Control Engineering, National Chiao Tung University, Hsinchu 300, Taiwan

M.-H. Chung
Department of Mechanical Engineering, Chung-Yuan Christian University, Chung-Li 320, Taiwan

1 Introduction

Optical disk drives serve as most common data-reading platforms nowadays for CD-ROM, DVD, CDP, LDP, etc. Inside the drives, the optical pickup is one of key components, which consists of objective lens on a movable bobbin (the lens holder) in order to achieve ultra-precision positioning of the lens for a better data-reading quality. As the demand for faster data-reading and density amounts is increased recently, the improvement of the speed and precision in the optical pick-up is needed. To achieve the goals, this study designs a dual-stage servo system, along with H_∞ and repetitive controls to perform a fast and precise data-tracking of optical disc drives.

The design aim of the tracking-following system in optical disk drives is to achieve desired control performance and robustness against modeling uncertainties and extraneous disturbance. The robust H_∞ control is capable of finding a feedback controller that guarantees robust performance and robust stability. Lee et al. (1996) developed robust H_∞ control with regional stability constrains for the track-following system of optical disk drive. Lim and Jung (1997) designed a H_∞ controller for an optical pick-up installed in 8× speed CD-ROM drive, and demonstrated that the controller has improved tracking performance. Kang and Yoon (1998) designed a robust control of an active tilting actuator for high-density optical disk. Choi et al. (1999, 2001) proposed a positioning control scheme for optical disc drives, using piezoceramic-based smart structures. In order to pursue the trend towards higher track densities and data rates in rotating memory devices, it requires track-following servo systems to own an increased bandwidth for reliable storage and retrieval of data.

One approach to overcome the problem is by using a dual-stage servo system. This dual-stage controller was

however initially applied to hard disc drives. In the servo proposed in this study, the voice coil motor (VCM) is used at a first stage to generate extensive but coarse and slow positioning, while the piezoactuator is used as a secondary stage to provide fine and fast positioning. Research works have been paid in the past decade to develop a mature dual-stage controller. Mori et al. (1991) proposed a dual-stage actuator using a piezoelectric device, while Hernandez et al. (1999) designed another dual-stage track-following servo controller for hard disc drives. Chung et al. (2000) also proposed a two-degree-of-freedom dual-stage actuator for hard disc drives, while Kobayashi and Horowitz (2001) also forged a dual-stage control for tracking and seeking. Recently for theoretically development of the dual-stage control, Zhang et al. (2008) developed an initial error shaping (IES) method for fast settling of the dual-stage controller, while Zheng and Fu (2008) proposed a nonlinear feedback controller in the structure of dual-stage for reducing settling time. As to the application of the dual-stage control to optical disk drives, it was dated back to 1996, when Yang and Pei (1996) proposed a basic dual-stage controller to optical pickup positioning. Cho et al. (2002) developed a swing-arm-type PZT dual actuator with fast seeking via self-sensing actuation (SSA) and positive position feedback (PPF) for optical disk drives. Ryoo et al. (2002) developed a dual-stage controller for precisely positioning the optical pick, using PQ method. In this study, a novel control is designed based on the μsynthesis technique and structure (Zhou and Doyle 1998), and mostly importantly a repetitive control capability is later added into the controlled system to deal with periodic disturbance caused by the rotation of an imbalanced optical disk. The above-mentioned repetitive control was utilized by Moon et al. (1998) for a tracking-following servo of an optical disk drive, while later applied to an ultrasonic motor in Kobayashi et al. (1999) in combination of H_∞ control. Zhong et al. (2002) also designed electronic converters to implement the repetitive control.

Owing to common practical limitations on actuators used in optical disc drives; e.g., physical bandwidths of actuators/sensors and limited control effort offered, this study proposes a dual-stage controller including a fast piezoceramic parallel-beam as a fine actuator and a VCM as a coarse one. The positioning algorithm would then consist of a robust H_∞ fine/coarse controllers designed based on μ synthesis and a repetitive controller to further reduce effects of disturbance on the positioning performance, which is often the main obstacle in CD/DVD control task. Note that in the control designed herein, the H_∞ dual and repetitive controllers share the task of reducing the disturbance caused by disc imbalance. Modeling is first conducted based experimental identification; then, the control design is followed. Simulations are next conducted to verify the effectiveness of the controllers designed and finally experiments are performed validate originally intended of the controllers.

In the next section, the modeling for the pick-up actuator is presented. In Sect. 3 the H_∞ controller is designed. Experimental results are subsequently presented in Sect. 4. Finally conclusions are given in Sect. 5.

2 Modeling via Identification

The dynamic models for the parallel-beam piezoceramic actuator and VCM are derived in this section, via experimental identification. A photo and its configuration of the piezoactuator are depicted in Fig. 1, which is made of piezoceramic parallel-beam. Figure 2, on the other hand, shows the VCM in the whole dual-stage actuator, which consists of the VCM and the piezoactuator. A PZT suspension is mounted at the end of the primary VCM arm.

For ensuing control design, the transfer function of this piezo-actuator is derived via an experiment system, for which a dynamic signal analyzer is used to obtain the frequency response of the piezoactuator first as subjected to

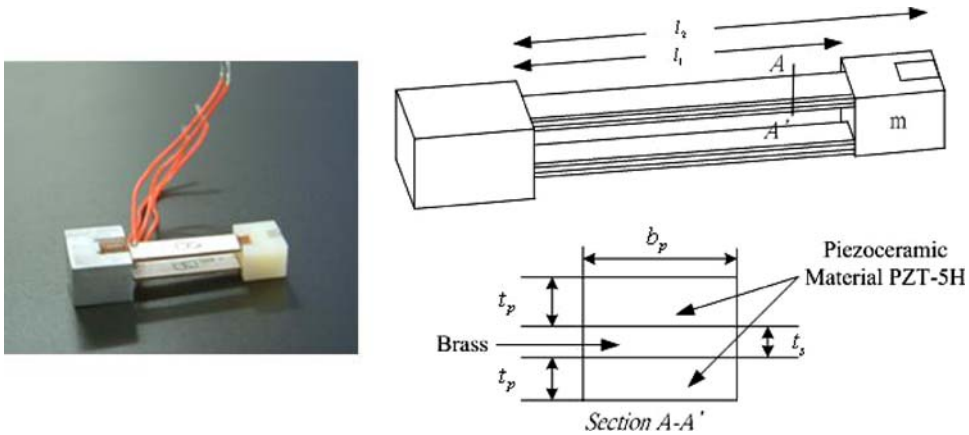

Fig. 1 The designed optical pick-up using piezoceramic bimorph structure

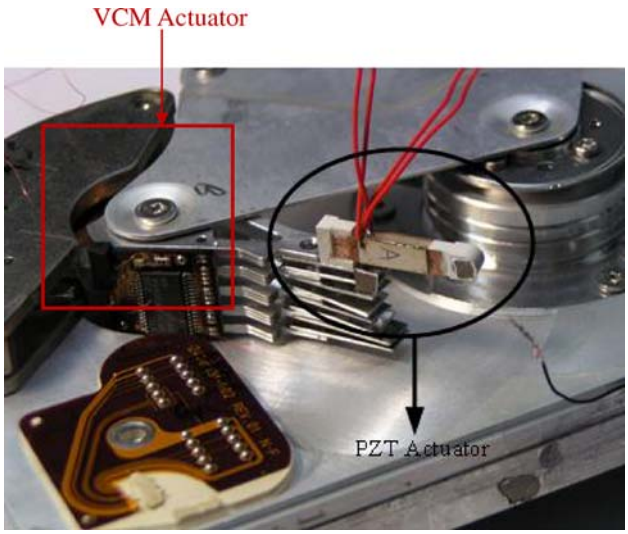

Fig. 2 The realistic dual-stage actuator for experimental validation

a swept sine excitation ranging from 5 Hz to 50 kHz. A laser displacement sensor measures the displacement of the objective lens tip and feedbacks the signal to the dynamic signal analyzer. The frequency response in bode diagram can be obtained. Figure 3 shows the result, where the first dynamic mode of the real system is considered and approximated for later control design. The forms of system transfer function to be identified is considered as (Choi et al. 1999, 2001).

$$G(s) = \frac{k\omega_n^2}{s^2 + 2\zeta\omega_n s + \omega_n^2}. \tag{1}$$

where ω_n, ζ and k are the nature frequency, the damping ratio and DC gain, respectively. The natural frequency can be directly identified from peak location of the experimental response in Fig. 3, which is approximately 297 Hz. The damping ratio ζ can be calculated by the following equation based on the response obtained, as shown in Fig. 3,

$$|G(j\omega)|_{\max} = \frac{1}{2\zeta\sqrt{1-\zeta^2}}. \tag{2}$$

The gain k was computed by the DC gain observed from Fig. 3 by the following equation

$$\text{DC gain} = 20\log\left|\frac{k\omega_n^2}{s^2 + 2\zeta\omega_n s + \omega_n^2}\right|_{s=j0}. \tag{3}$$

Therefore, the system transfer function can be identified by a common computation process of curve-fitting, yielding

$$G_{\text{PZT}}(s) = \frac{4.912 \times 10^5}{s^2 + 144.9s + 3.93 \times 10^6}\left(\frac{\mu\text{m}}{\text{volt}}\right). \tag{4}$$

The identified system frequency response is also shown in Fig. 3, where it is seen that the responses of the real system and the identified two-order system are closely matched before 3,000 rad/s, which is normally beyond the actuation bandwidth of a piezo-actuator.

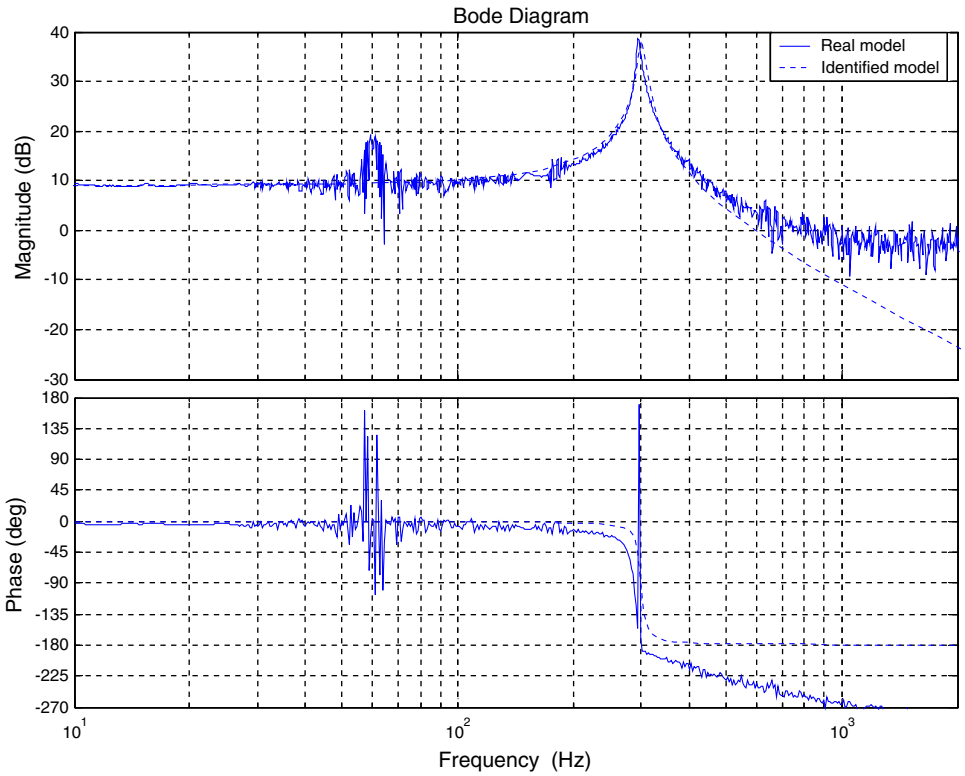

Fig. 3 Frequency responses of the real and identified model

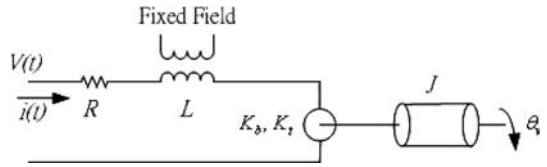

Fig. 4 The univalent circuit of the VCM actuator

Table 1 VCM system parameters

V_{VCM}	Control voltage
$i(t)$	Work current
$\theta_v(t)$	VCM angle displacement
R	VCM resistance
L	VCM inductance
K_b	Counter-electromotive force
K_t	VCM torque constant
J	Moment of inertia

The VCM in the dual-stage motor is next identified. The VCM is subjected to an electric voltage as an input. Figure 2 shows the realistic experimental system for dual-stage control, where though it is actually built in a hard drive, ready to be implemented in an optical disk drive. The associated equivalent circuit is shown in Fig. 4 and the associated parameter definitions are listed in Table 1. From basic electromagnetic behavior of this VCM, the input–output dynamics can be modeled by a third-order transfer function of the form

$$\frac{\theta_v(s)}{V_{\text{VCM}}(s)} = \left[\frac{1}{s\left(\frac{LJ}{K_t}s^2 + \frac{RJ}{K_t}s + K_b\right)}\right]. \tag{5}$$

A dynamic signal analyzer is next used to obtain the input–output dynamic response, which is shown in Fig. 5, along with a curve-fitted response to match the experimental counterpart. The resulted identified transfer function of VCM is

$$G_{\text{VCM}}(s) = \frac{2\times 10^{10}}{s(s+80)(s+9,000)}\left(\frac{\mu\text{m}}{\text{volt}}\right). \tag{6}$$

3 Control design

The ensuing control design process consists of three stages: (1) a baseline PI/double-lead compensator and robust H_∞ controller for the piezoactuator, (2) a robust H_∞ dual-stage controller for VCM and piezo-actuator, (3) a repetitive controller for the dual-stage actuator.

3.1 Control design for the piezoactuator

The conventional PI-and-double-lead compensator and H_∞ controller are designed in this section, with a performance comparison between them. The PI-and-double-lead compensator is employed for its simple structure, while the H_∞ controller for inherent robustness.

3.1.1 PI-and-double-lead compensator

A well-designed phase-lead compensator is capable of achieving desired stability and transient response. With the desired compensated phase angle designated over 60°, the double-lead compensator is often employed. On the other hand, to annihilate steady-state error completely for the Type 0 system of the piezoactuator, the PI controller is augmented to the pre-designed double-lead compensator. Thus, the PI/double-lead compensator is of the form

$$C_{\text{PDL, PZT}}(s) = K\frac{1}{s}\frac{1+\tau_1 s}{1+\alpha_1\tau_1 s}\frac{1+\tau_2 s}{1+\alpha_2\tau_2 s} \tag{7}$$
$$K>0,\ \ \tau>0,\ \ 0<\alpha<1,$$

where the subscript "PDL" denotes "PI-and-double-lead." The PI-and-double-lead compensator must satisfy the time-domain specifications as

$$T_s = 0.05\,\text{s},\quad M_p = 0.05,\quad \text{PM} > 60^\circ, \tag{8}$$

where T_s, M_p and PM are settling time, maximum overshoot and phase margin, respectively. Note that the control specifications in Eq. 8 are focused on the larger-range seeking control of the optical pickup with precision—about 10 μm positioning. This is expected to be achieved within approximate 50 ms (=T_s) with little maximum overshoot; $M_p = 0.05$; and small oscillation; PM > 60°. These specifications are compatible to those in (Cho et al. 2002). Following the fundamental process for designing lead compensator in (Palm 1986), the PI-and-double-lead compensator can be successfully designed as

$$G_c(s) = 362.3646\frac{(0.0016s+1)(0.0012s+1)}{(0.0001s+1)(0.0001s+1)}. \tag{9}$$

The frequency response of the compensated open-loop system is depicted and shown in Fig. 6. The phase margin is clearly 62.4°, which satisfies the original performance specifications for the system.

3.1.2 H_∞ controller

The H_∞ control structure employed is shown in Fig. 7, where the exogenous inputs and controlled outputs are regulated by five weighting functions. In this figure, z_1 is the error signal; z_2 is the controlled signal; d is the disturbance signal; n is the noise signal; u is the control input;

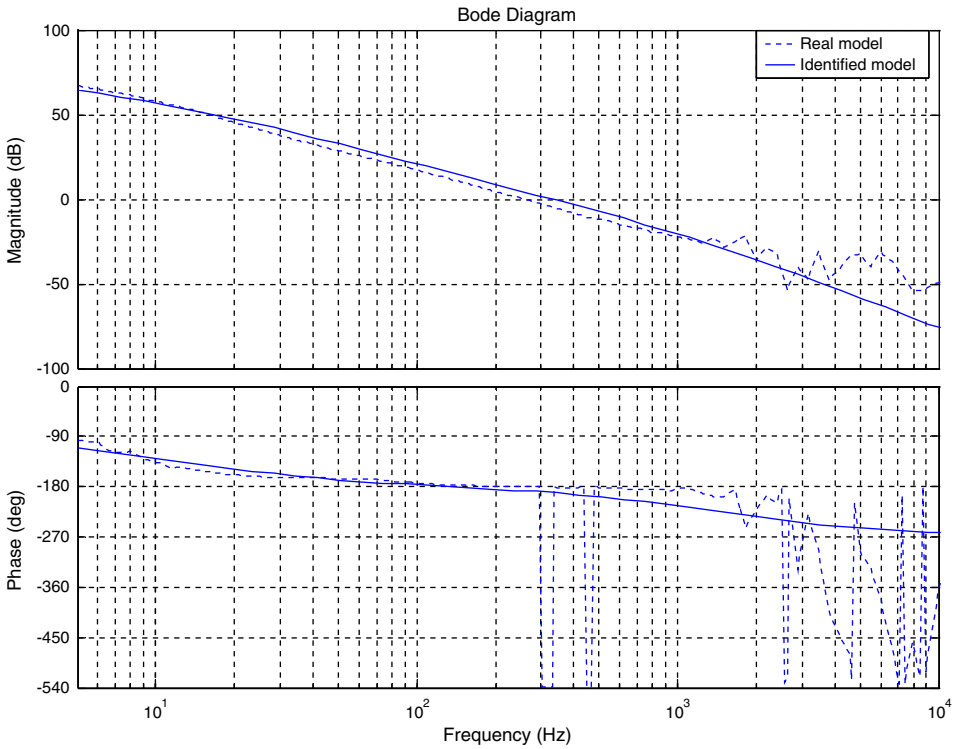

Fig. 5 Frequency responses of the real and identified model

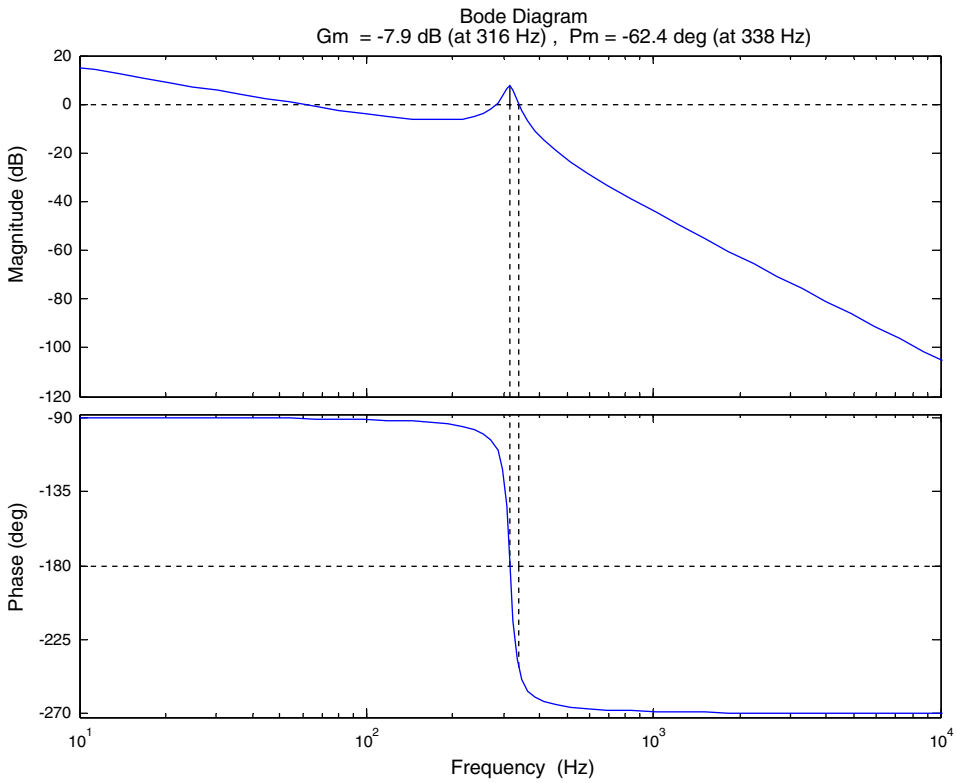

Fig. 6 Bode plot of the system compensated by the PI-and-double-lead controller

r is the reference signal; P is the plant; K is the controller; W_e reflects the requirements on control objective; W_u does some restrictions on the control or actuator signals; W_d and W_n are designed to reject the disturbances and noises, respectively; W_a is the multiplicative uncertainty weighting function; Δ is the multiplicative uncertainty. A typical design process of a H_∞ control design (Hernandez et al. 1999) is initialized by determining the aforementioned

weighting functions, which affect the system sensitivity function, control sensitivity function and complementary sensitivity functions that are used to examine if the originally set performance specifications are satisfied. The determination of five weighting functions for the piezoactuator is detailed in the followings.

1. Performance weighting function W_e.

Based on the structure in Fig. 7, in order to reject the effect of external disturbance on the error, the magnitude of sensitivity function must be kept small over the considered bandwidth. The sensitivity function S and complementary sensitivity function T are defined as follows,

$$S = \frac{1}{1+PK} \quad \text{and} \quad T = \frac{PK}{1+PK}. \tag{10}$$

The weighting function W_e can be selected to satisfy $\|W_e S W_d\|_\infty \le 1$ by the small gain theorem, which leads to the design of W_e as

$$W_e = \frac{s/M_s + \omega_b}{s + \omega_b \varepsilon_e}, \tag{11}$$

where

$$M_s = \|S\|_\infty = |S(j\omega_{\max})| = \frac{\Omega\sqrt{\Omega^2 + 4\zeta^2}}{\sqrt{(1-\Omega^2)^2 + 4\zeta^2\Omega^2}}, \tag{12}$$

$$\Omega = \sqrt{0.5 + 0.5\sqrt{1+8\zeta^2}}, \quad \omega_{\max} = \Omega\omega_n, \quad \omega_b \approx \omega_n/\sqrt{2}. \tag{13}$$

For practical purpose, one can usually choose a suitable ε_e as shown in Fig. 8a that is related to the steady-state error. Choosing $\varepsilon_e = 0.001$ leads to

$$M_p = 0.05(\le 5\%), \quad T_s = 0.01\,\text{s}. \tag{14}$$

With determined time-domain performance specifications T_s and M_p, $\{\zeta, \omega_n\}$ can be calculated, and then $\{\omega_b, M_s\}$ from Eqs. 12 and 13, completing the design of the performance weighting function W_e.

2. Control-restricting weighting function W_u.

The determination of control weighting function W_u is based on the control signal equation

$$u = KS(r - n - d). \tag{15}$$

where r is the input reference, n is the sensor noise, d is the input disturbance. The magnitude of $|KS|$ in the low-frequency range is essentially limited by the allowable cost

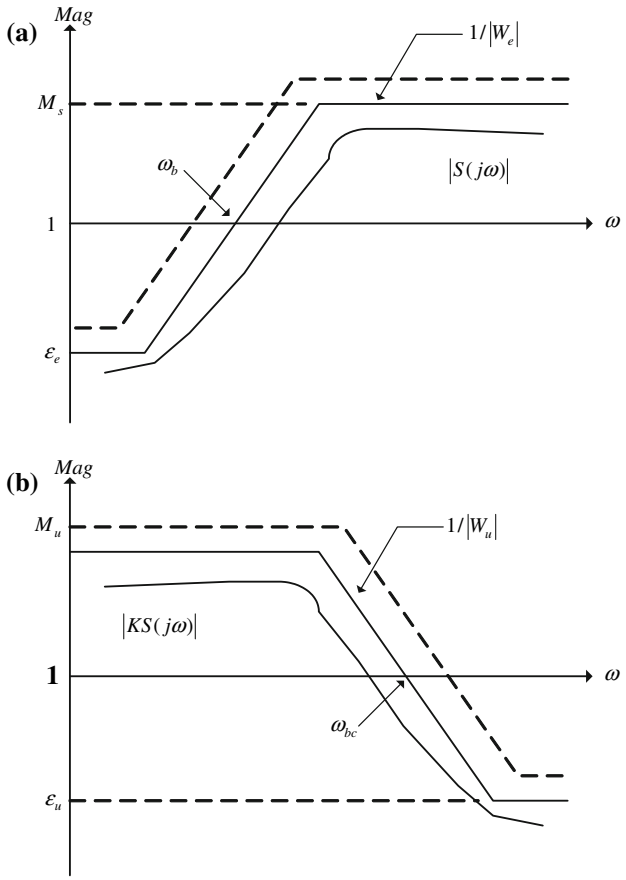

Fig. 8 Frequency responses of **a** performance weight W_e and desired S, **b** control weight W_u and desired KS

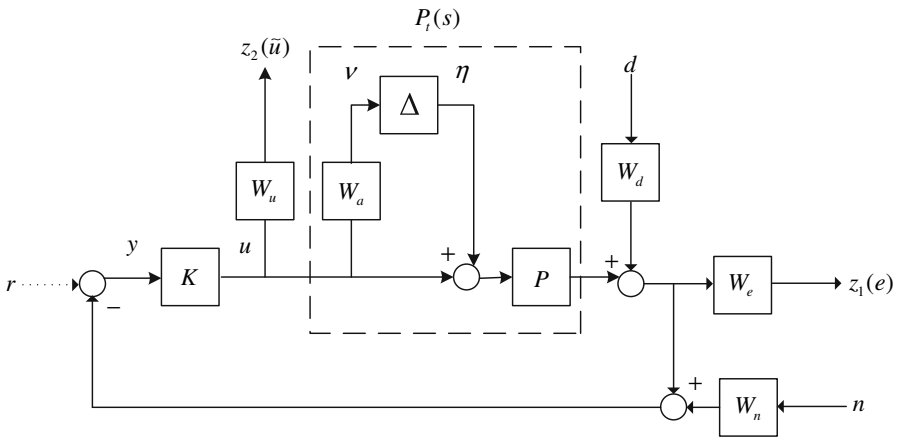

Fig. 7 The H_∞ control design structure

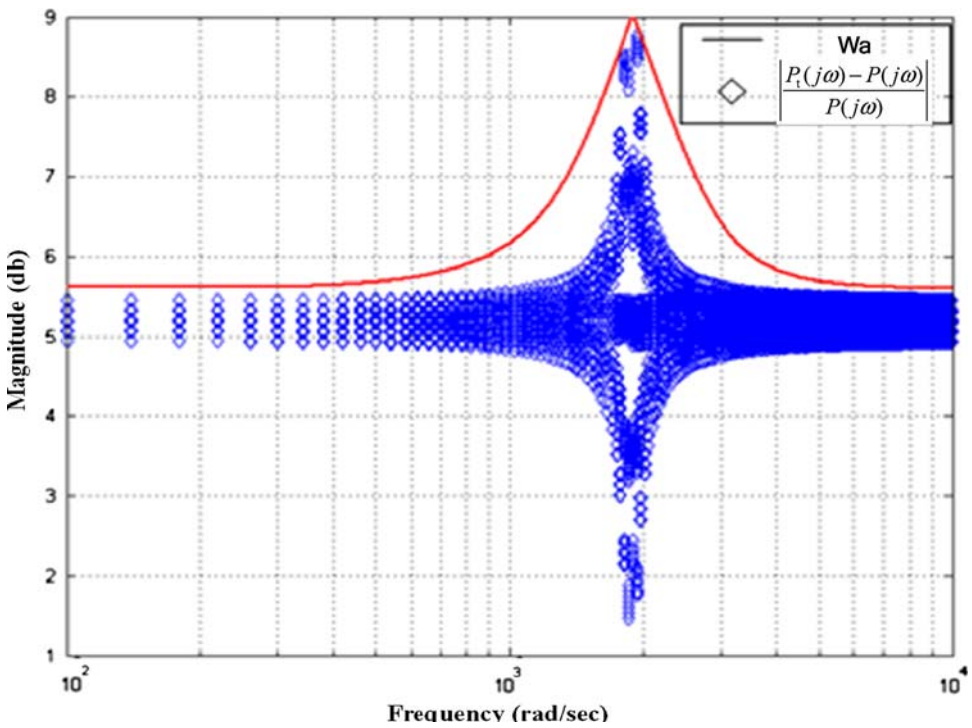

Fig. 9 $\left|\frac{P_t(j\omega)-P(j\omega)}{P(j\omega)}\right|$ and the bond W_a

of control effort and saturation limit of the actuators; henceforth, the maximum gain of KS, denoted by M_u, ought to be designed large, while the high-frequency gain is essentially limited by the controller bandwidth frequency of the beam ω_{bc} and the sensor noise frequency. The candidate weight W_u can be designed of the form (Zhou and Doyle 1998)

$$W_u = \frac{s + \omega_{bc}/M_u}{\varepsilon_u s + \omega_{bc}}. \tag{16}$$

For the present study, M_u is designated as 90, which is the maximum input voltage to the piezoactuator, while the bandwidth frequency of the beam, $\omega_{bc} = 2{,}000$ Hz, is designated as the controller bandwidth frequency. In the next step, as shown in Fig. 8b, a suitable ε_u is chosen to satisfy $\|W_u KSW_d\|_\infty \leq 1$ by the small gain theorem, which is set as 0.75.

3. Disturbance weighting function W_d.

Consider the disturbance caused by eccentric rotation of the disk, when a disk is rotated at a high-speed state. In this case, by using the MATLAB signal processing toolbox, the disturbance weighting function W_d can be designed as a Butterworth bandpass filter with the two cut-off frequencies set as the disk rotating speeds that were between 1,800 and 2,100 rpm. Therefore, the disturbance weighting function is

$$W_d = \frac{100.5s}{s^2 + 100.5s + 983{,}000}. \tag{17}$$

4. Sensor noise weighting function W_n.

The noise weighting function W_n is used to penalize sensor noise that is caused by laser displacement sensor,

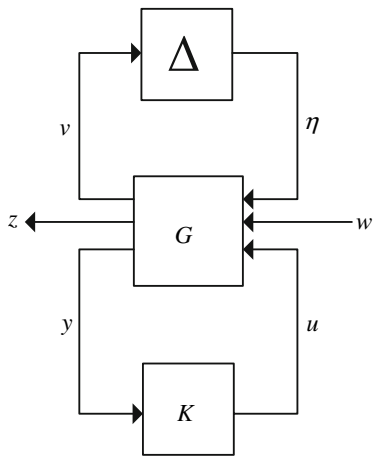

Fig. 10 The LFT framework of the H_∞ control considering plant uncertainty

wires and environmental stimulation that are relatively significant at some high frequencies. To this aim, W_n is selected to be a high-pass filter to reflect the effect of the aforementioned noise on the system performance. Based on measurement noises, the cut-off frequency is set as 5 Hz to capture sensor noise. Therefore, the noise weighting function can designed of the form

$$W_n = \frac{s}{s + 31.42}. \tag{18}$$

5. Multiplicative uncertainty weighting function W_a.

The difference between identified model and the real model is called "uncertainty". There are two different

kinds of uncertainties. One is structured uncertainty, while another is unstructured one. The former reflects the variations in every uncertain parameter of the system; for example, the manufacture tolerance value during mass production. The latter refers to those other than the parametric uncertainty, such as unknown high-order dynamics in this study. The difference between the identified model and the real model will be modeled to be structured uncertainty with the multiplicative weighting function W_a designed to bond the plant uncertainty. The block diagram for modeling the plant uncertainty was shown in Fig. 7, where $P_t(s)$ indicates the completely description of the plant with variation 1%. The weighting function W_a can be calculated by the following equation

$$|W_a(j\omega)| \geq \left|\frac{P_t(j\omega) - P(j\omega)}{P(j\omega)}\right| \forall \omega. \tag{19}$$

With required computation based on Eq. 19 at each frequency, W_a can be captured by

$$W_a = \frac{0.026211(s^2 + 2685s + 3.47e6)}{s^2 + 193.9s + 4{,}037{,}000}. \tag{20}$$

Figure 9 shows the Bode diagram of plant uncertainty, where it is seen that $|(P_t(j\omega) - P(j\omega))/P(j\omega)|$ has been well upper-bounded by W_a at all frequencies.

Prior to H_∞ control design in the next subsection, the structure in Fig. 7 is transformed into an LFT framework as shown in Fig. 10, for a standard μ synthesis to design the H_∞ controller. In Fig. 10, G is the interconnection matrix; K is the controller; w is a vector signal including noises and disturbances; z is a vector signal including all controlled signals and tracking errors; Δ is the set of all possible uncertainty; u is the control signal; y is the measurement. A comparison between Figs. 7 and 10 leads to

$$\begin{bmatrix} \nu \\ z_1 \\ z_2 \\ y \end{bmatrix} = G(s) \begin{bmatrix} \eta \\ d \\ n \\ u \end{bmatrix} \Leftrightarrow \begin{bmatrix} \nu \\ z_1 \\ z_2 \\ y \end{bmatrix} = \left[\begin{array}{ccc|c} 0 & 0 & 0 & -W_a \\ PW_e & W_eW_d & 0 & -PW_e \\ 0 & 0 & 0 & -W_u \\ \hline P & W_d & W_n & -P \end{array}\right] \begin{bmatrix} \eta \\ d \\ n \\ u \end{bmatrix}.$$

The goal of a standard H_∞ control design is to find all admissible controllers $K(s)$ such that the exogenous input to controlled output transfer function $\|T_{z\omega}\|_\infty$ is minimized. However, it is difficult to find an absolutely optimal H_∞ controller, since it is both numerically and theoretically complicated. In practice, it is often not necessary to design an optimal H_∞ controller, rather a so-called sub-optimal H_∞ controller that can be solved and suit well the control goal to some degree (Zhou and Doyle 1998). With the plant uncertainty considered, an H_∞ controller of order 16 can be found with the input/output transfer function satisfying $\|T_{zw}\|_\infty \leq 0.9774$. Model reduction is also performed to reduce the order the controller to 9, yielding

$$K(s) = \frac{4393.1023(s + 16760)(s + 502.7)(s^2 + 39.48s + 39{,}940)(s^2 + 144.9s + 3{,}930{,}000)(s^2 + 193.9s + 4{,}037{,}000)}{(s + 11{,}840)(s + 496.7)(s + 0.6857)(s^2 + 31.41s + 41{,}450)(s^2 + 196.7s + 4{,}049{,}000)(s^2 + 7329s + 33{,}580{,}000)}. \tag{22}$$

With the above H_∞ controller designed successfully, two conditions are examined to ensure robust performance and robust stability, respectively, in

$$\left\| \begin{matrix} W_eSW_d \\ W_uKSW_d \end{matrix} \right\| \leq 1 \tag{23}$$

for robust performance, and

$$\|W_aKS\| \leq 1 \tag{24}$$

for robust stability with multiplicative uncertainty considered. Figure 11 shows the simulated performance indices defined in the LHS of Eqs. 23 and 24, where it is seen that the robust performance criteria and stability as given in Eqs. 23 and 24 are satisfied.

3.2 Design of the dual-stage controller

An H_∞ controller is designed next for a dual-stage servo system, which consists of a parallel-beam piezoceramic structure as the fine actuator and a VCM as the coarse actuator. Figure 12 shows a block diagram of the decoupled dual-stage servo system. The head position y_T is a combination of the VCM output y_V and the PZT output y_P. The output of the PZT actuator is added to the input of the VCM controller, which prevents the PZT actuator from going to the end of its stroke limit and maintains the output of the PZT on the center of the track. The closed-loop transfer function from a reference r to the head position y_T is given by

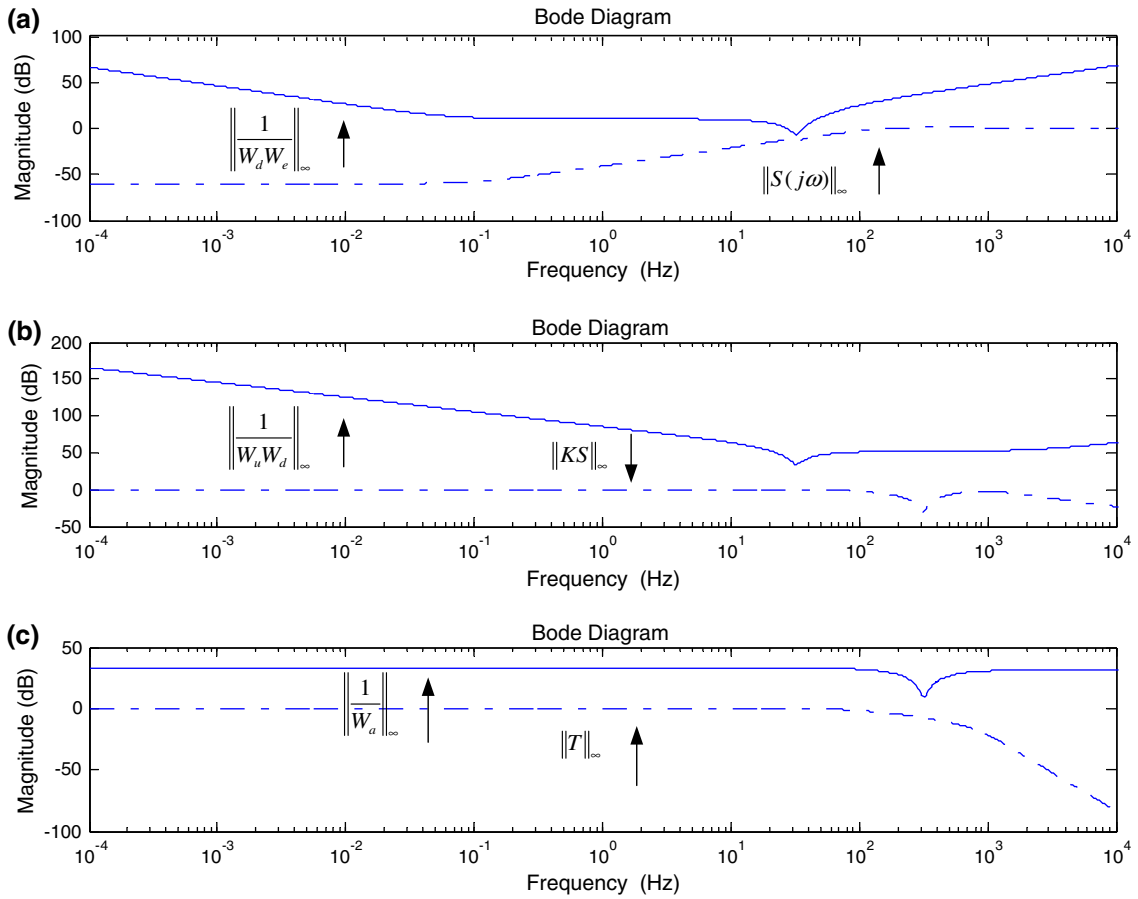

Fig. 11 **a** Robust performance, **b** Robust performance, **c** Robust stability

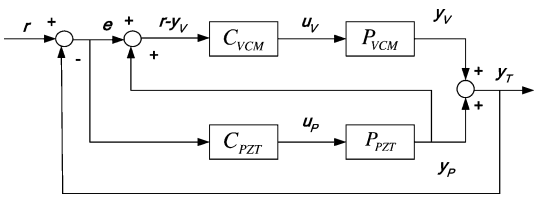

Fig. 12 The block diagram of decoupled track-following design

$$y_T = \frac{P_{\mathrm{VCM}}C_{\mathrm{VCM}}(1 + P_{\mathrm{PZT}}C_{\mathrm{PZT}}) + P_{\mathrm{PZT}}C_{\mathrm{PZT}}}{(1 + P_{\mathrm{VCM}}C_{\mathrm{VCM}})(1 + P_{\mathrm{PZT}}C_{\mathrm{PZT}})} r, \tag{25}$$

where P_{VCM} and P_{PZT} are the plants for VCM or PZT actuators, respectively. C_{VCM} and C_{PZT} are the associated controllers to be designed. The sensitivity function S_T is

$$S_T = \frac{e}{r} = \frac{1}{(1 + P_{\mathrm{VCM}}C_{\mathrm{VCM}})(1 + P_{\mathrm{PZT}}C_{\mathrm{PZT}})}. \tag{26}$$

In the above equation, the total sensitivity function of the decoupled servo system is the product of the VCM and PZT loop sensitivity. Thus, the controller design can be decoupled into two independent controller designs, the VCM loop and PZT loop.

The framework of μ synthesis in a block diagram is employed next for design of the dual-stage servo controller, as shown in Fig. 13, which is a easy result of direct transformation from Fig. 12. This block diagram contains various signals and weightings that allow for a complete description of a dual-stage CD-ROM control system. P_{VCM} and P_{PZT} denote the nominal plants of the coarse VCM and fine PZT actuators, respectively. Independent multiplicative or additive uncertainty can be used to describe uncertainty for both the coarse actuator and piezoactuator. $W_{\mathrm{VCM\_un}}$ and $W_{\mathrm{PZT\_un}}$ denote the multiplicative uncertainties for them, respectively. Several disturbance signals are accounted for in the model, including (1) input disturbances to the coarse and fine actuators, d_{VCM} and d_{PZT}, respectively; (2) the VCM sensor noise n_{VCM} and the piezoactuator sensor noise n_{PZT}. The weightings W_{VCM_d}, W_{PZT_d}, W_{VCM_n} and W_{PZT_n} are corresponding frequency shaping filters. These weightings must be selected by the designer with sufficient fidelity. The signals for design in the synthesis model are the VCM position signal, the piezoactuator relative position signal, the VCM control input and piezoactuator control input. These signals are, respectively, multiplied by scaling factors W_{VCM_e}, W_{PZT_e},

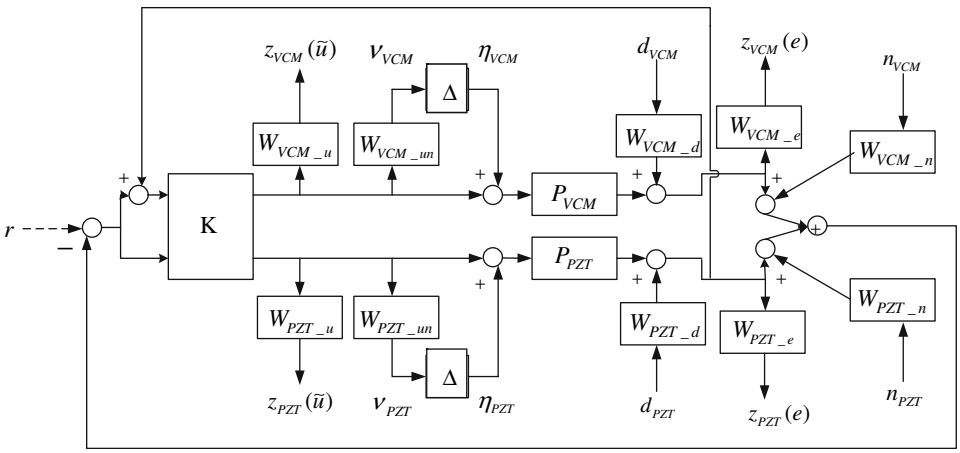

Fig. 13 The block diagram of H_∞ dual-stage control

Table 2 Weightings

Weight	Transfer function
$W_{\text{VCM\_}e}$	$\frac{0.65s+31.02}{s+0.03102}$
$W_{\text{PZT\_}e}$	$\frac{0.7796s+79.92}{s+0.07992}$
$W_{\text{VCM\_}u}$	$\frac{s+3142}{0.001s+3142}$
$W_{\text{PZT\_}u}$	$\frac{s+139.6}{0.75s+1.257\times10^4}$
$W_{\text{VCM\_d}}$	$\frac{1005s}{s^2+100.5s+9.83\times10^5}$
$W_{\text{PZT\_}d}$	$\frac{100.5s}{s^2+100.5s+9.83\times10^5}$
$W_{\text{VCM\_}n}$	$\frac{s}{s+31.42}$
$W_{\text{PZT\_}n}$	$\frac{s}{s+157.1}$
$W_{\text{VCM\_un}}$	$\frac{0.02586s+13.08}{s+456.8}$
$W_{\text{PZT\_un}}$	$\frac{0.02215s^2+113.3s+2.605\times10^5}{s^2+319.2s+1.201\times10^7}$

$W_{\text{VCM\_}u}$ and $W_{\text{PZT\_}u}$ to forge the performance output signals $z_{\text{VCM}}(e)$, $z_{\text{PZT}}(e)$, $z_{\text{VCM}}(\tilde{u})$ and $z_{\text{PZT}}(\tilde{u})$. Table 2 lists all designed weightings used in the μ synthesis block diagram for H_∞ control design in Fig. 13.

Given a set of input and output weightings and plant uncertainties, the μ synthesis is performed successfully and then a controller is synthesized which results in a singular value less than or equal to 1. An H_∞ controller of order 16 can be found with the input/output transfer function satisfying $\|T_{zw}\|_\infty \leq 0.9861$. Order reduction is also performed to reduce the order of the controller to 9, yielding the H_∞ controller of the form

$$\begin{bmatrix} \frac{0.14659(s+3.142\times10^6)(s+9{,}000)(s+456.8)(s+80)(s+31.42)(s+0.5598)(s^2+82.09s+8.101\times10^5)}{(s+3.853\times10^4)(s+456.8)(s+0.4537)(s^2+0.8757s+4.366)(s^2+100.5s+9.83\times10^5)(s^2+3.823e4s+1.433\times10^9)} \\ 0 \end{bmatrix}$$
$$\begin{bmatrix} 0 \\ \frac{170.7858(s+1.676\times10^4)(s+157.1)(s^2-53.11s+8.405\times10^5)(s^2+234.6+1.19\times10^7)(s^2+319.2s+1.201\times10^7)}{(s+1{,}311)(s+164.3)(s+0.09294)(s^2+64.49s+9.484\times10^5)(s^2+330.5s+1.201\times10^7)(s^2+971.1s+1.312\times10^7)} \end{bmatrix}. \quad (27)$$

Utilization of the controller in Eq. 27, the overall sensitivity function S_T can be plotted, as seen in Fig. 14, where S_T has further attenuation compared to the sensitivity function S_{VCM} of VCM loop.

3.3 Design of repetitive control

Periodic disturbance exist due to the rotation of an imbalanced optical disk. These disturbances are around the rotational speed, 155 Hz, for the present study. Owing to the inability of an H_∞ controller to counteract periodic disturbances, a repetitive compensator is designed and augmented to the H_∞ dual-stage controller in order to suppress the negative effects of the periodic disturbance on the control performance. Figure 15 shows the newly designed system involving the H_∞ dual-stage controller and the repetitive compensator. The repetitive compensator is designed to be composed of a low-pass filter

$$F(s) = \frac{\omega_c}{s+\omega_c}, \quad (28)$$

and a time delay e^{-Ls} where L is slightly less than the period of external position disturbance L_d; i.e.,

$$L = L_d - \frac{1}{\omega_c}. \quad (29)$$

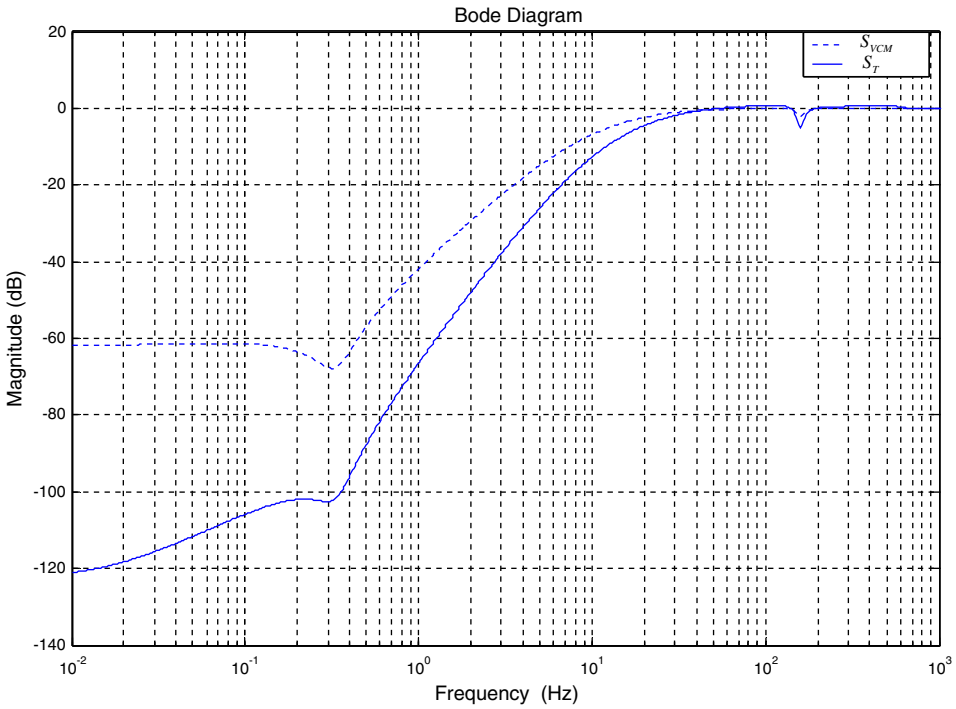

Fig. 14 Frequency responses of sensitivity functions

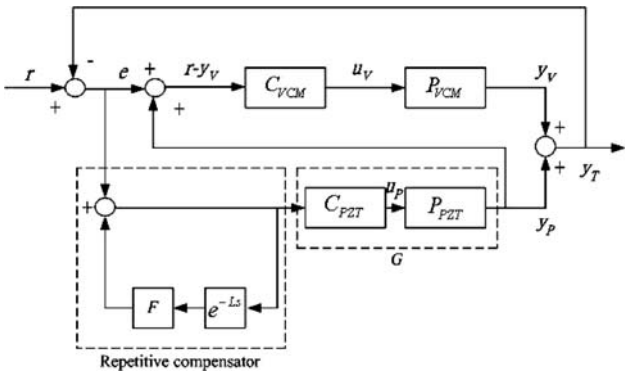

Fig. 15 The H_∞ dual-stage controller with the repetitive compensator

Assume that the transfer function $G(s)$: $= P_{\mathrm{PZT}}(s)\, C_{\mathrm{PZT}}(s)$ has no unstable pole-zero cancellation. Then, the repetitive control system shown in Fig. 15 is internally stable if the following two conditions hold (Kobayashi et al. 1999):

i. H_∞ control system depicted in Fig. 12 is internally stable;
ii. $|F\ (j\omega)| < |1 + G\ (j\omega)|\ \forall\ \omega \in R$.

The above condition (i) has already been satisfied since $C_{\mathrm{PZT}}(j\omega)$ is a controller solution from Eq. 27 based on H_∞ control design theory. The low-pass filter $F\ (s)$ in condition (ii) should be appropriately selected for good tracking performance without resultant instability. If the choice of ω_c is too low, only few poles of the internal model are close to the imaginary axis, leading to poor tracking. If ω_c is too high, the system is difficult to stabilize; thus, $F\ (s)$ is chosen as

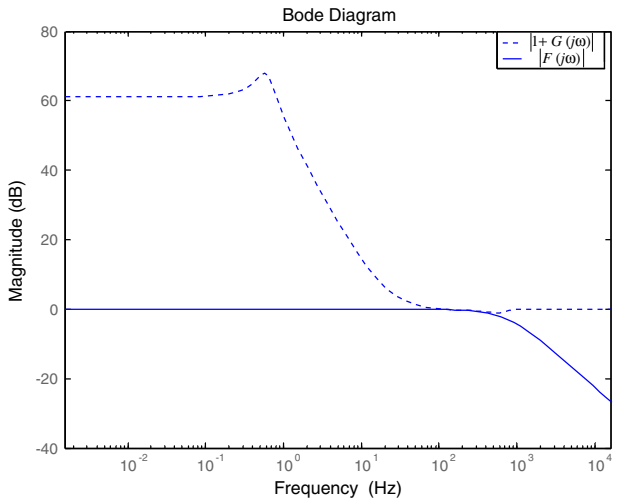

Fig. 16 Gain of the low-pass filter $F(s)$ and $1 + G(s)$

$$F(s) = \frac{\omega_c}{s + \omega_c}, \quad \omega_c = 2\pi \times 750\,\mathrm{rad/s} \tag{30}$$

for satisfying condition (ii). Figure 16 shows $|F(j\omega)|$ as the solid curve and $|1 + G(j\omega)|$ as the dotted curves, where it is clearly seen that the above-mentioned condition (ii) is satisfied for all frequencies.

4 Experiment verification

The previous control designs are applied to the realistic dual-stage actuator as shown in Fig. 3 for performance test

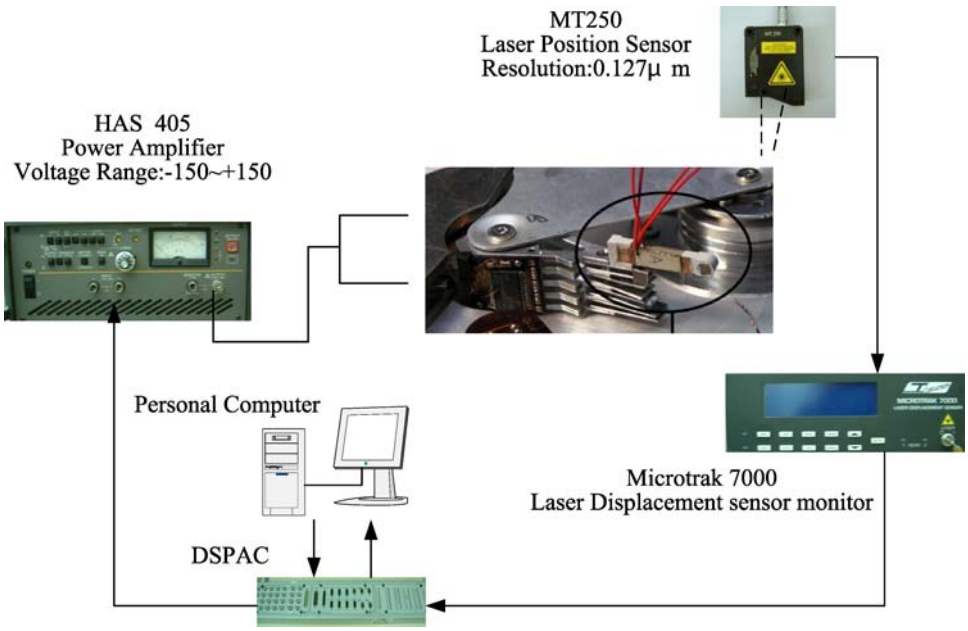

Fig. 17 Experimental framework for controller performance validation

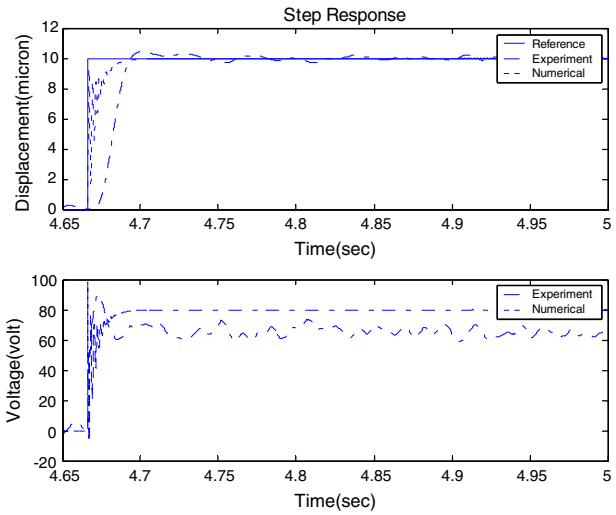

Fig. 18 Experimental and numerical results for the PI-and-double-lead compensator

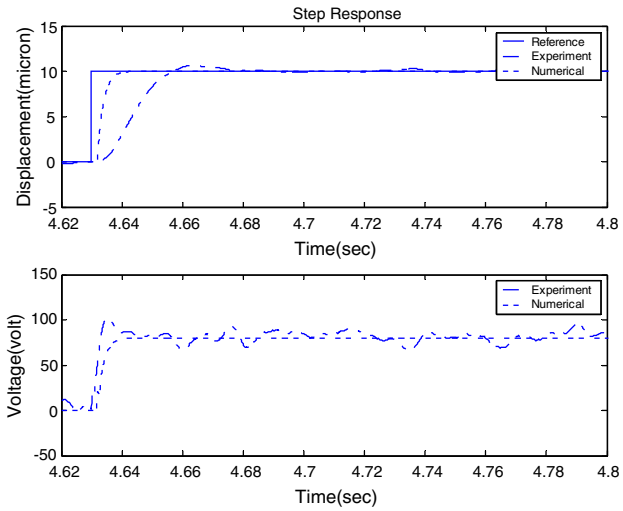

Fig. 19 Experimental and numerical results for the H_∞ control considering plant uncertainty

and the comparison to that by a traditional PI-and-double-lead compensator. Figure 17 shows the experiment framework. The implementation of the control algorithms is accomplished by a dSPACE module. The output control signal is amplified by a power amplifier (HAS 4051) to provide enough voltage to move the actuator. The motion of the objective lens is measured by a laser displacement sensor (MTI 250, MICROTRAK 7000). The sensor signal is feedbacked to dSPACE module for computing the control output. Note that the resolution of the laser displacement is around ±0.2 μm.

Figures 18 and 19 show experimental results along with simulated counterparts for step control of the piezo-actuator. The controllers employed are PI-and-double-lead compensator and H_∞ controller for comparison. It is seen from these figures that both controllers need about 0.04 s to settle in a 10 μm step with indistinguishable steady-state errors. However, the PI-and-double-lead controller needs higher voltage than simulation data to reach 10 μm at steady state. This is probably due to the nonlinear phenomenon called ''creep'' (Kuhnen and Janocha, 1998), which changes gradually the static relationship between the displacement and applied voltage. Also, some fluctuations present in all steady-state displacements in both Figs. 18 and 19 are caused by the measurement error of laser displacement sensor since the resolution of laser displacement sensor is about ±0.5 to 0.6 μm.

In addition to the above qualitative observation, efforts are paid to conduct quantitative analysis, which is initiated by defining the "averaged error" as

$$E_p = \frac{\sum_1^n |y_{\text{exp}} - y_{\text{des}}|}{n}, \tag{31}$$

where n is the number of the experiment samples, y_{exp} is the experimental data, and y_{des} is the desired trajectory, i.e., a step responses. E_p is thus an indication of control performance. For the experimental data presented in Figs. 18 and 19, the values of E_p are 0.2226 and 0.2433 μm, respectively, for H_∞ and the PI-and-double-lead compensators, showing a better performance by the H_∞ control. Also noted is that the experimental averaged errors of the two controllers are closer to the resolution of laser displacement sensor, indicating that both controllers have pushed the performance to natural limit.

Attention now turns to the performance validation of the dual-stage controller. Figure 20 shows the experimental and numerical step responses of the closed-loop system with the dual-stage controller in Eq. 27 applied in subfigure (a); individual displacements actuated by VCM and PZT in subfigure (b); control efforts in subfigures (c) and (d). It is seen from subfigure (a) that the controller is capable of reaching 8 μm at steady state, despite the fluctuating displacements and control efforts by the VCM and piezo-actuators, respectively seen in subfigures (b) and (c). These fluctuations, particularly magnified in subfigure (e), are caused by the in-precision coarse VCM actuator. It is compensated by the fine piezo-actuator, which is evidenced by the experimental smooth step response seen in subfigure (a) and out-of-phase displacements seen from subfigure (e).

Figure 21 shows the steady-state experimental and simulated step response error and control effort subjected

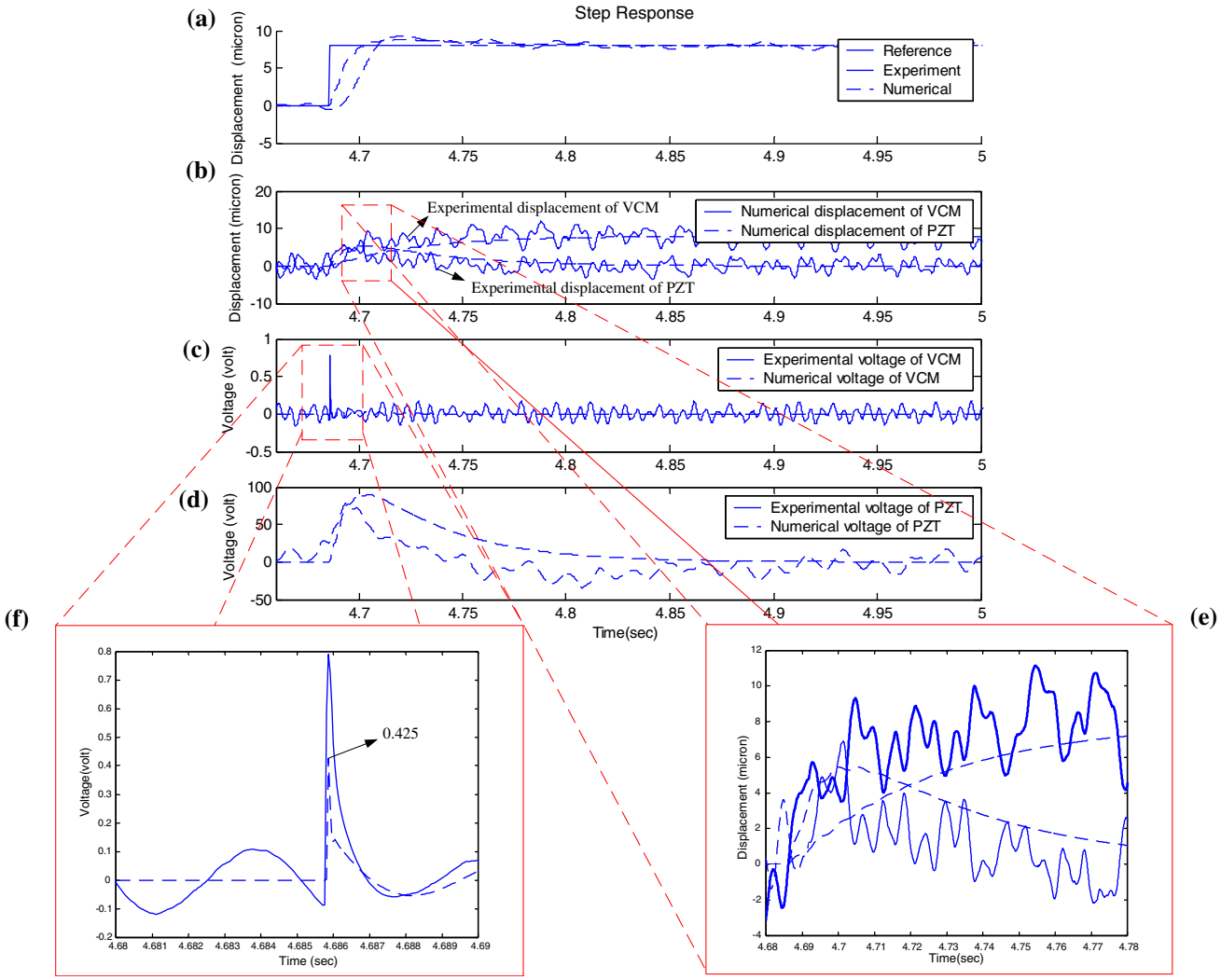

Fig. 20 Experimental and numerical results for the H_∞ dual-stage control

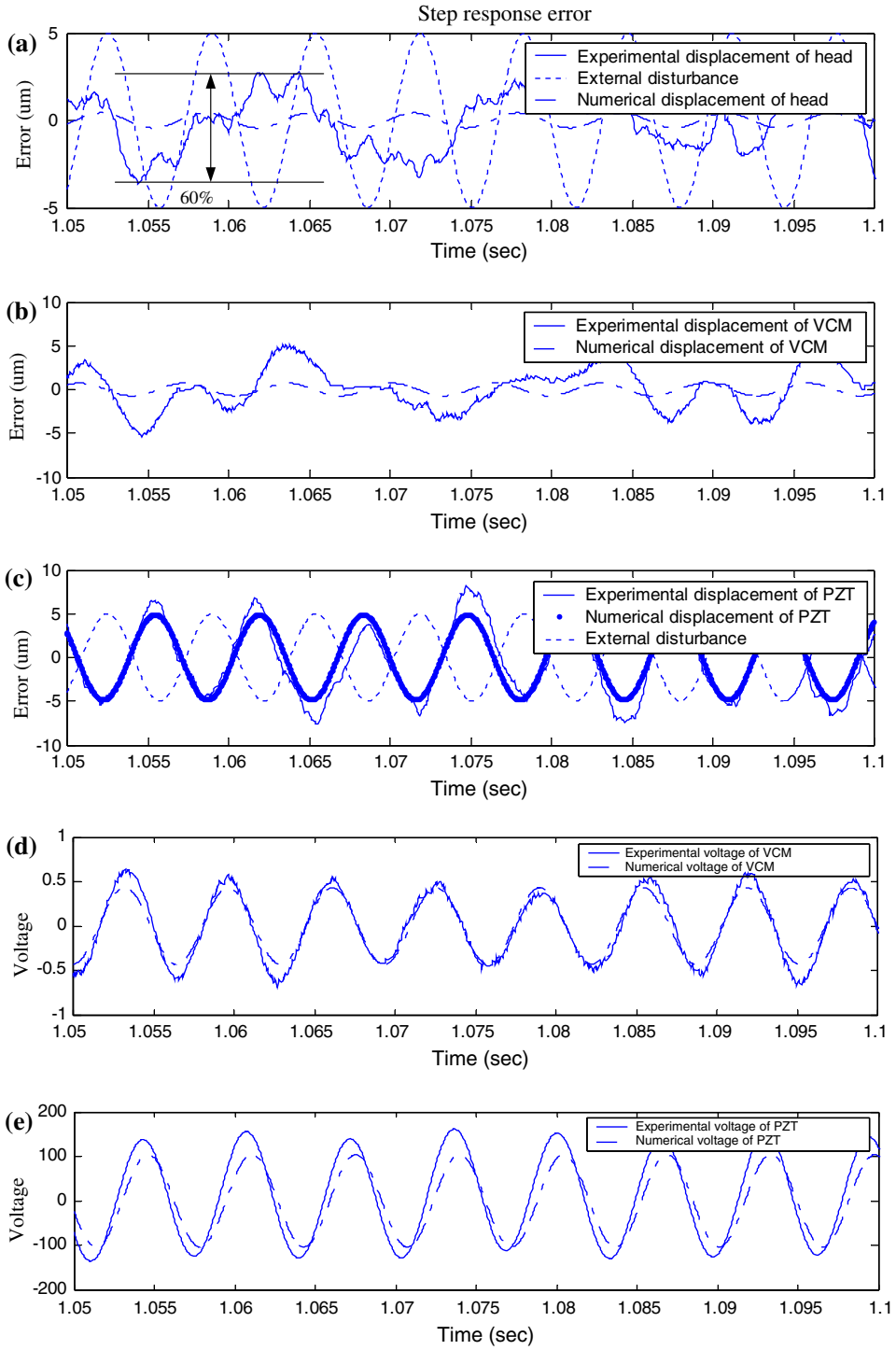

Fig. 21 Experimental and numerical results for the H_∞ dual-stage control with repetitive control while considering the disturbance at 155 Hz

to sinusoidal input, where an external 155 Hz disturbance in the level of 5 μm is added at the output for testing the performance of the repetitive controller. It is seen from subfigure (a) that the external disturbance in the level of 5 μm is suppressed 0.5 and 3 μm, respectively, for numerical and experimental results, showing the effectiveness of designed H_∞ dual-stage and repetitive controller. In other words, the H_∞ dual-stage controller with repetitive control can reject the disturbance up to 40% of the original. On the other hand, subfigures (b) and (c) show the positioning errors by VCM and piezo-actuator. It is noted that substantial positioning error is observed from subfigure (b), which is due to in-precision mechatronic characteristics of the coarse VCM actuator. This is also evidenced from the mismatch between experimental and numerical data in subfigure (d). Fortunately, it is seen from

subfigure (c) that the fine piezo-actuator successfully exerts the response out of phase to the intentionally added external disturbance, resulting in relatively smaller error response in subfigure (a). In a short conclusion from observation on Figs. 20 and 21, the fine piezo-actuator bears the responsibilities of compensating in-precision positioning of the coarse VCM actuator and external small level periodic disturbance.

5 Conclusion and future work

A new dual-stage lens actuator based on the H_∞ control and repetitive control is proposed in this study for an optical pickup in optical disk drives. The coarse and fine actuations are implemented by VCM and piezo-actuators. Dynamic modelings of both actuators are first conducted via experimental identifications. The controllers of the traditional PI-and-double-lead and H_∞ dual-stage controller are subsequently designed for precision positioning. The effectiveness of the designed controllers are finally demonstrated based on experimental studies. The designed controller is demonstrated capable of achieving the precision seeking in 0.04 s and suppressing an external 155 Hz disturbance in the level of 5 μm up to 40% of the original. It is found from experimental and numerical data that the fine piezo-actuator bears the responsibilities of compensating in-precision positioning of the coarse VCM actuator and external small level periodic disturbance.

It should be noted that the choice of $F(s)$-filter in repetitive control hinders the capability of the repetitive controller to precisely predict the primary period and phase of the disturbance. In the future, an adaptive-like $F(s)$-filter should be designed for repetitive control.

Acknowledgments The authors are greatly indebtzed to the National Science Council of R.O.C. for the supports via the research contracts in nos. of NSC 96-2200-E-009-029 and NSC 97-2221-E-009-057-MY3.

References

Cho WI, Park NC, Yang H, Park Y-P (2002) Swing-arm-type PZT dual actuator with fast seeking for optical disk drive. Microsyst Technol 8:139–148

Choi SB, Cho SS, Park YP (1999) Vibration and position tracking control of piezoceramic-based smart structures via QFT. ASME J Dyn Syst Meas Control 121:27–32

Choi SB, Kim HK, Lim SC, Park YP (2001) Position tracking control of an optical pick-up device using piezoceramic actuator. Mechatronics 11:691–705

Chung CC, Seo CW, Lee SH (2000) Two degree-of-freedom dual-stage actuator controller design for hard disk drives. IEEE Trans Magn 36:2255–2257

Hernandez D, Park SS, Horowitz R (1999) Dual-stage track-following servo design for hard drive. Proc Am Control Conf 6:4116–4121

Kang JY, Yoon MG (1998) Robust control of an active tilting actuator for high-density optical disk. Proceedings of American Control Conference, pp 861–865

Kobayashi M, Horowitz R (2001) Track seek control for hard disk dual-stage servo system. IEEE Trans Magn 37:949–954

Kobayashi Y, Kimura T, Yanabe S (1999) Robust speed control of ultrasonic motor based on H_∞ control with repetitive compensator. JSME Int J Ser C 42:884–890

Kuhnen K, Janocha H (1998) Compensation of the creep and hysteresis effects of piezoelectric actuators with inverse systems. Proceedings of the 6th International Conference on new actuators, Bremen, September, pp 309–312

Lee MN, Moon JH, Chung MJ (1996) Robust H_∞ control with regional stability constrains for the track-following system of optical disk drive. Proc. IECON'96, pp 1388–1393

Lim SC, Jung TY (1997) Robust servo control of high speed optical disk drives. Proceedings of the Korean Society for noise and vibration engineering, pp 438–444

Moon JH, Lee MN, Chung MJ (1998) Repetitive control for the track-following servo system of an optical disk drive. IEEE Trans Control Syst Technol 6:663–670

Mori K, Munemoto T, Otsuki H, Yamaguchi Y, Akagi K (1991) A dual-stage magnetic disk drive actuator using a piezoelectric device for a high track density. IEEE Trans Magn 27:5298–5300

Palm WJIII (1986) Control systems engineering. Wiley, Canada

Ryoo JR, Doh T-Y, Chung MJ (2002) Compensator design for a dual-stage actuator in the track-following servo system of optical disk drives. IEEE Trans Consumer Electron 51:471–477

Yang JD, Pei XD (1996) Seek time and trajectories of time. Optimal control for a dual stage optical disk drive actuator. IEEE Trans Magn 32:3857–3859

Zhang J, Du C, Ge SS (2008) A novel settling controller for dual-stage servo systems. IEEE Trans Magn 44:3757–3760

Zheng JH, Fu MY (2008) Nonlinear feedback control of a dual-stage actuator system for reduced settling time. IEEE Trans Control Syst Technol 16:717–725

Zhong QC, Green T, Liang J, Weiss G (2002) Robust repetitive control of grid-connected DC-AC converters. IEEE Conference on Decision and Control, pp 2468–2473

Zhou K, Doyle JC (1998) Essentials of robust control. Prentice-Hall, New Jersey